AIMS Mathematics, 8(2): 4682–4699.
DOI: 10.3934/math.2023231
Received: 06 October 2022
Revised: 17 November 2022
Accepted: 24 November 2022
Published: 06 December 2022

http://www.aimspress.com/journal/Math

Research article

Combine influence of Hall effects and viscous dissipation on the motion of ethylene glycol conveying alumina, silica and titania nanoparticles using the non-Newtonian Casson model

Umar Nazir and Kanit Mukdasai*

Department of Mathematics, Faculty of Science, Khon Kaen University, Khon Kaen 40002, Thailand

* **Correspondence:** Email: kanit@kku.ac.th.

Abstract: A vital role of ternary hybrid nanofluid is visualized as a significant improvement of thermal performance and enhancement in thermal rate which is applicable in automobiles for coolant process, thermodynamics of fuel. This process of ternary hybrid nanofluid is utilized to enhance maximum performance of thermal energy and applicable in chemical products, solar power, melting process, wire paintings, biological products, solar system, cooling process, glasses melting, glass fiber, metal grinding etc. Three-dimensional motion of ternary hybrid nanoparticles in partially Casson fluid over a vertical stretching surface is addressed using Darcy's Forchheirmer theory. Further, effects of Joule heating, non-uniform thermal radiation and viscous dissipation are considered in the energy equation and motion of ethylene glycol contains alumina, silica, and titania nanoparticles with various shape effects. Similarity variables are utilized to derive the system of ODEs from PDEs. A system of ODEs is numerically solved by a finite element method. It was concluded that the thermal field for platelet nanoparticles is greater than the thermal field for cylindrical nanoparticles. Nusselt number increases versus change in ion slip, Hall and magnetic parameters. Maximum production of heat energy is obtained for the case of tri-hybrid nanomaterial rather than for the case of hybrid nanomaterial.

Keywords: Hall and ion slip forces; ternary hybrid nanofluid; various shapes of nanoparticles; vertical surface; FEM; Forchheirmer porous model
Mathematics Subject Classification: 65L10, 76A02, 76D05

List of symbols:

W, V, U	Velocity components (ms^{-1})	y, x, z	Space coordinates (m)
ν	Kinematic viscosity (m^2s^{-1})	β	Casson fluid number
ρ	Fluidic density (Kgm^{-3})	β_i, β_e	Ion slip and Hall parameters
T	Temperature (K)	T_∞	Ambient temperature (K)
μ	Viscosity $(Kgm^{-1}s^{-1})$	G	Gravitational acceleration (N)
β, γ	Buoyancy parameters	B_0	Magnetic induction $(A.Kgs^{-2})$
σ	Electrical conductivity (Sm^{-1})	n	Power law index number
a, b	Constants	T_w	Wall temperature (K)
η	Independent variable	Pr	Prandtl number
M	Magnetic number	ϕ_3, ϕ_1, ϕ_2	Volume fractions
λ	Stretching ratio number	Cf	Skin friction coefficient
Nu	Nusselt number	TH	Tri-hybrid nanofluid
bf	Base fluid	EG	Ethylene glycol
Al_2O_3	Aluminum oxide	SiO_2	Silicon dioxide
w_1, w_3, w_2, w_4, w_5	Weight functions	∞	Infinity
K	Thermal conductivity (Wm^{-1})	PDEs	Partial differential equations
ODEs	Ordinary differential equations	sp_1, sp_3, sp_2	Solid nanoparticles
θ_ω	Temperature ratio number	N_r	Thermal radiation number
ϵ	Porosity parameter (m^2)	f_s	Inertia coefficient
k^1	Permeability of porous (m^2)	F_r	Forchheimer number
σ^*, k^*	Stefan-Boltzmann constants	α	Thermal diffusivity (m^2s^{-1})

1. Introduction

Nanofluid is an engineered colloidal mixture regarding base fluid with single nanoparticles. Such behavior of fluid is applicable in cooling process, thermal process, thermal enhancement, thermal reduction and microelectronics. Deep exploration regarding case of mixture of base fluid with two kind's nanoparticles is termed as hybrid nanofluid. Moreover, Casson fluid behaves like a non-Newtonian liquid and shear thinning. Such type of non-Newtonian rheology is applicable in petroleum products, syrup drugs, production of plastic materials and engineering field etc. Rheology related to Casson fluid was investigated by Casson [1]. He has investigated that Casson model displays role like a shear thinning, plastic liquid model and high shear viscosity. Chabani et al. [2] discussed features of hybrid nanoparticles involving Lorentz force in triangular enclosure. They have studied convective flow considering the Darcy Forchheimer model and included that flow is reduced when Lorentz force is implemented. Chu et al. [3] investigated a study related to hybrid nanofluid in the presence of magnetohydrodynamics for unsteady flow in two parallel plates including shape effects. They considered engine oil as base fluid and model is numerical solved by numerical scheme. Selimefendigil et al. [4] studied the role of various shapes regarding nanoparticles in ventilated cavities considering artificial neural networks. They implemented a finite element approach to find numerical results. It was included that maximum temperature was obtained using L-shaped cavity. Saleem et al. [5] estimated performance of several shapes of nanoparticles in horizontal surface considering base fluid (water). They have used a shooting approach to find parametric study on temperature and flow profiles. It was established that mass transport rate is enhanced versus erratic motion. Saleem et al. [6] established

modeling related to Eyring-Powell material considering magnetized effect in mass species and heat transfer involving chemical reaction using finite element approach. Algehyne et al. [7] studied thermal features of Maxwell fluid in hybrid particles over a stretching frame. They have utilized finite element approach to find computational study and parametric study. It was investigated that highest thermal performance can be achieved by hybrid nanofluid rather than nanofluid. Imran et al. [8] performed thermal aspects of the solar collector using approach of hybrid nanoparticles via several shape effects implementing a numerical approach. Several studies regarding hybrid nanofluid are mentioned in [9]. Khan et al. [10] discussed features of Lorentz force in Casson fluid inserting dust particles along with hybrid nanoparticles past a stretchable sheet using an analytic approach.

Ternary hybrid nanofluid is a mixture of three kinds of nanoparticles in base fluid. It is an efficient approach to achieve the highest temperature rather than nanofluid and hybrid nanofluid. The process regarding tri-hybrid nanoparticles is most efficient for development of thermal enhancement and thermal reduction. Sarada et a. [11] estimated enhancement process in energy efficient using applications of ternary hybrid nanoparticles in curved stretching sheet implementing shooting approach. Nazir et al. [12] visualized comparison enhancement into different fluids using Hall currents inserting mixture of multiple nanoparticles in base fluid via finite element methodology. Dezfulizadeh et al. [13] discussed impacts of Lorentz force in MHD flow using exergy an efficiency approach in the presence of ternary hybrid nanofluid. Oke [14] determined performance of tri-hybrid nanofluid in mass dissuasion and thermal energy considering base fluid (EG) past a rotating surface. Xiu et al. [15] studied dynamic behavior of ternary-hybrid nanoparticles in mass diffusion and thermal field considering small and large volume of nanoparticles with platelet, spherical and cylindrical nanoparticles over wedge using shooting approach. They have found that tri-hybrid nanofluid was observed very significantly for thermal performance rather than hybrid nanofluid. Animasaun and Asogwa [16] discussed comparative influences among alumina and water-based nanoparticles including based cupric nanoparticles (water-based) over stretching surface. Rasool et al. [17] experienced multiple aspects based on radiation and viscous dissipation using theory of non-Fourier's in second grade rheology using analytic approach on porous surface. Ashraf et al. [18] captured thermal features of magnetohydrodynamic flow in peristaltic fluid inserting magnetite nanoparticles in blood using the D-quadrature algorithm.

Nowadays, several industrial applications in pigments, electronics, cosmetics, food processing and utilizing engineering process metal oxide nanomaterials such as silicon dioxide, aluminum oxide and titanium dioxide. The retention and transport of nanoparticles (Al_2O_3, SiO_2, TiO_2) ware utilized to resolve issues of petroleum engineering and environmental. Nanoparticles (Al_2O_3, SiO_2, TiO_2) were introduced for enhancement of oil recovery by Hendraningrat et al. [19]. Al_2O_3 nanoparticles have higher boiling and melting points which are useful for enhancement of thermal inertia (see Song et al. [20]). In addition, Al_2O_3 nanoparticles are applicable to enhance the strengthens of smoothness, ceramics, creep resistance and crack hardness. Dynamic features of thermal transport in the presence of partially ionized liquid subjected to magnetic field is significantly exaggerated by magnetic field. Animasaun et al. [21] investigated that the Hall effect occurs when a magnetic field is applied perpendicular to the current flow through a thin sheet. As a result, an electric field is created parallel to the magnetic and current fields and directly proportional to the product of the magnetic induction and current density. Animasaun et al. [22] discussed comparison impacts among 47 nm and 36 nm alumina nanoparticles in base fluid (water) under action of Hall currents. Farooq et al. [23] developed model of entropy production rate in mass diffusion and thermal field under effects of Hall currents,

viscous dissipation, magnetic field and Joule heating in cylindrical tubules.

The purpose of the present flow problem is to study characterizations of Casson fluid involving Lorentz force and thermal radiation (non-linear) over a 3D vertical surface accompanied with buoyancy force, Forchheimer porous model and Joule heating. In additionally, mixture of three kinds of nanoparticles (Al_2O_3, SiO_2, TiO_2) in ethylene glycol is inserted to visualize thermal performance among cylindrical and platelet nanoparticles. The current problem fills the gap while not adequately studied with the following points.

- Analysis of heat transfer in Casson liquid under effects of Joule heating and viscous dissipation, thermal radiation (non-linear), Hall and ion slip forces using Darcy's Forchheimer theory past a 3D surface has not been investigated yet.
- Previous to this investigation, no comparative analysis on Casson fluid among cylindrical and platelet nanoparticles over 3D surface using Forchheimer porous model has been existed in literature works computed by finite element method.
- In existence literature, no investigations have been reported including ternary hybrid nanoparticles and shape effects rather than [24] to visualize comparative analysis among cylindrical and platelet nanoparticles.

Existence works demonstrate that development of Casson liquid inserting ternary hybrid nanofluid using thermal properties of various shapes of nanoparticles over 3-dimensional vertical using Forchheimer porous model frame is not studied yet. Moreover, ion slip and Hall currents are considered with viscous dissipation and variable thermal conductivity. Present complex development is numerically handled by a finite element approach. In addition, section I, section II, section IV and section V are based on literature review, problem modeling, numerical approach, results and conclusions, respectively.

2. Modeling of developed model

A 3D model of Casson fluid is developed over a stretching surface using theories of generalized Ohm's law and Darcy's Forchheimer model. Three types of nanoparticles are inserted into EG (ethylene glycol) while various shapes of nanoparticles (cylindrical and platelet) are addressed. Motion of nanoparticles is produced using movement of wall velocity. Buoyancy force is considered whereas viscous dissipation and thermal radiation (non-linear) are added in the energy equation. Suspension of nanoparticles regarding aluminum oxide, titanium oxide and silicon dioxide in working fluid is considered. Reduced form regarding Navier-Stoke equations is obtained and physical model is considered by Figure 1. Thermal radiation in terms of non-linear is utilized to determine thermal fields. Surface is assumed as non-conducting in terms of electrically and non-isothermal. Figure 1 is 3D vertical surface in y-, x- and z-components while non-uniform magnetic field is considered along z-component and gravitational force acts along downward direction. Partially flow over surface is induced by bidirectional movement of wall velocities U_w and V_w at $z = 0$. A 3D surface lies in plane at $z = 0$ and flow occupies region in field at $z > 0$. Wall temperature and ambient temperature are considered as T_w and T_∞. Further, it is studied that ethylene glycol is shear thinning [25], non-Newtonian liquid [26] and plasma [26]. Casson fluid model is also known as non-Newtonian liquid and shear thinning [1]. Table 1 reveals thermal properties of various nanoparticles. So, its rheology is prescribed by the Casson fluid stress tensor relation.

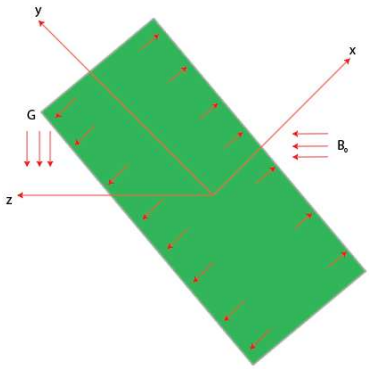

Figure 1. Physical representation of 3D model.

Table 1. Thermal conductivity, density and electrical conductivity in EG [27].

	k	ρ	σ
Al_2O_3	32.9	6310	5.96×10^7
SiO_2	1.4013	2270	3.5×10^6
TiO_2	8.953	4250	2.4×10^6
EG	0.144	884	0.125×10^{-11}

Conservation laws for energy equation, momentum equation for incompressible and steady flow [24] using Casson liquid are

$$U_x + V_y + W_z = 0, \tag{1}$$

$$UU_x + VU_y + WU_z = \frac{\mu_{TH}}{\rho_{TH}}\left(1 + \frac{1}{\beta}\right)U_{zz} - \frac{\mu_{TH}}{\rho_{TH}}f_s U - \frac{f_s}{(k^1)^{1/2}}U^2$$

$$+\frac{(B_0)^2(y+x)^{n-1}\sigma_{TH}}{\rho_{TH}[(1+\beta_i\beta_e)^2+\beta_e^2]}[\beta_e V - (1+\beta_e\beta_i)U] + G\beta_{TH}(T - T_\infty), \tag{2}$$

$$UV_x + VV_y + WV_z = \frac{\mu_{TH}}{\rho_{TH}}\left(1 + \frac{1}{\beta}\right)V_{zz} - \frac{\mu_{TH}}{\rho_{TH}}f_s V - \frac{f_s}{(k^1)^{1/2}}V^2$$

$$-\frac{(B_0)^2(y+x)^{n-1}\sigma_{TH}}{\rho_{TH}[(1+\beta_i\beta_e)^2+\beta_e^2]}[\beta_e U + (1+\beta_e\beta_i)V] + G\gamma_{TH}(T - T_\infty), \tag{3}$$

$$UT_x + VT_y + WT_z = \frac{(B_0)^2(y+x)^{n-1}\sigma_{TH}}{\rho_{TH}[(1+\beta_i\beta_e)^2+\beta_e^2]}(U^2 + V^2) + \left(\alpha T_z + \frac{16T^3\sigma^*}{3k^*(\rho C_p)_f}T_z\right)_z$$

$$+\frac{\mu_{TH}}{(\rho C_p)_{TH}}\left(1 + \frac{1}{\beta}\right)[(U_z)^2 + (V_z)^2], \tag{4}$$

Boundary conditions [24] of developing model are defined as

$$U = a(x+y)^n, V = b(x+y)^n, W = 0, as\ z = 0, U = 0,$$

$$T \to T_\infty, V = 0,\ \ as\ z \to \infty, T = T_w = T_\infty + A_1 T_0 (y+x)^{2n}. \tag{5}$$

Similarity variables [24] are delivered as

$$U = a(y+x)^n F', V = b(y+x)^n G', \eta = \sqrt{\frac{a}{\nu_f}}(y+x)^{\frac{n-1}{2}} z,$$

$$W = -\sqrt{a\nu_f}(x+y)^{\frac{n-1}{2}}\left\{\frac{n+1}{2}(F+G) + \frac{n-1}{2}\eta(F'+G')\right\}. \tag{6}$$

Equations (1)–(4) into dimensionless form [24] using variables similarity are

$$\left(1+\frac{1}{\beta}\right)F''' - A_1\left[-n(F'+G')F' + \frac{n+1}{2}(F+G)F''\right] - \epsilon F' - \frac{\nu_f}{\nu_{TH}} Fr F'^2$$

$$+\frac{M^2(1-\phi_1)^{2.5}(1-\phi_2)^{2.5}}{(1-\phi_3)^{-2.5}[(1+\beta_i\beta_e)^2+(\beta_e)^2]}[\beta_e G' - (1+\beta_e\beta_i)F'] + \alpha_1\theta = 0, \tag{7}$$

$$\left(1+\frac{1}{\beta}\right)G''' + A_1\left[n(F'+G')G' - \frac{n+1}{2}(F+G)G''\right] - \epsilon G' - \frac{\nu_f}{\nu_{TH}} Fr G'^2$$

$$-\frac{M^2(1-\phi_1)^{2.5}(1-\phi_2)^{2.5}}{(1-\phi_3)^{-2.5}[(1+\beta_i\beta_e)^2+(\beta_e)^2]}[\beta_e F' + (1+\beta_e\beta_i)G'] + \alpha_2\theta = 0, \tag{8}$$

$$\left((1+N_r(1+(\theta_\omega-1)\theta')^3)\right)' + \frac{k_f(\rho c_p)_{TH}}{k_{TH}(\rho c_p)_f} Pr\left[\frac{n+1}{2}\theta'(F+G) - n\theta(F'+G')\right]$$

$$+\frac{k_f}{k_{TH}}\frac{PrEcM^2}{(1+\beta_i\beta_e)^2+(\beta_e)^2}[(F')^2 + (G')^2] = 0, \tag{9}$$

BCs in term of dimensionless [24] are

$$F(0) = F'(\infty) = 0, F'(0) = 1, (0) = G'(\infty) = 0, G'(0) = \lambda, \theta(0) = 1 = 0, \theta(\infty) = 0. \tag{10}$$

Correlations regarding ternary hybrid nanofluid [28] for density, thermal conductivity and viscosity are defined as

$$A_1 = (1-\phi_1-\phi_2-\phi_3) + \phi_1\frac{\rho_{sp_1}}{\rho_f} + \phi_2\frac{\rho_{sp_2}}{\rho_f} + \phi_3\frac{\rho_{sp_3}}{\rho_f}, \tag{11}$$

$$\mu_{TH} = \mu_{Nf1}\phi_1 + \mu_{Nf2}\phi_2 + \mu_{Nf3}\phi_3, K_{TH} = \frac{K_{Nf1}\phi_1 + K_{Nf2}\phi_2 + K_{Nf3}\phi_3}{\phi}, \tag{12}$$

$$\rho_{TH} = (1-\phi_1-\phi_2-\phi_3)\rho_{bf} + \phi_1\rho_{sp_1} + \phi_2\rho_{sp_2} + \phi_2\rho_{sp_2}, \tag{13}$$

$$(\rho C_p)_{TH} = (1-\phi_1-\phi_2-\phi_3)(\rho C_p)_{bf} + \phi_1(\rho C_p)_{sp_1} + \phi_2(\rho C_p)_{sp_2} + \phi_3(\rho C_p)_{sp_3}, \tag{14}$$

Thermal conductivity and viscosity models for cylindrical and platelet (see Figure 2) [28] are defined

as

$$\frac{\mu_{Nf2}}{\mu_{bf}} = 1 + 904.4\phi^2 + 13.5\phi, K_{nf1} = K_{bf}\left[\frac{K_{sp_2}+3.9K_{bf}-3.9\phi\left(K_{bf}-K_{sp_2}\right)}{K_{sp_2}+3.9K_{bf}+\phi\left(K_{bf}-K_{sp_2}\right)}\right], \tag{15}$$

$$\frac{\mu_{Nf3}}{\mu_{bf}} = 1 + 612.6\phi^2 + 37.1\phi, K_{nf} = K_{bf}\left[\frac{K_{sp_3}+4.7K_{bf}-4.7\phi\left(K_{bf}-K_{sp_3}\right)}{K_{sp_3}+4.7K_{bf}+\phi\left(K_{bf}-K_{sp_3}\right)}\right]. \tag{16}$$

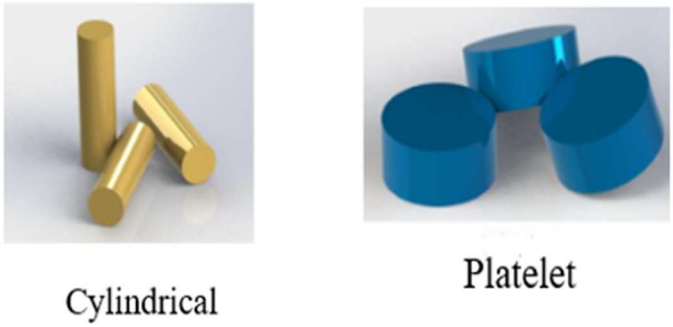

Figure 2. Representation of platelet and cylindrical nanoparticles.

Wall shear stresses due to ternary hybrid nanofluid [24] are derived as

$$Cf = \frac{\tau_{zx}|_{z=0}}{\rho_{TH}(u_w)^2}, Re^{1/2}Cf = \frac{(1+\phi_3)^{-2.5}(n+1)^{1/2}}{(1+\phi_2)^{2.5}(1+\phi_1)^{2.5}}\left(1+\frac{1}{\beta}\right)F''(0), \tag{17}$$

$$Cg = \frac{\tau_{zy}|_{z=0}}{\rho_{TH}(u_w)^2}, Re^{1/2}Cg = \frac{(1+\phi_3)^{-2.5}(n+1)^{1/2}}{(1+\phi_2)^{2.5}(1+\phi_1)^{2.5}}\left(1+\frac{1}{\beta}\right)G''(0). \tag{18}$$

Temperature gradient due to ternary hybrid nanofluid [24] is

$$Nu = \frac{-K_{TH}(y+x)T_z|_{z=0}}{(T_w-T_\infty)K_f}, NuRe^{-1/2} - \frac{K_{TH}}{K_f}\theta'(0). \tag{19}$$

3. Computational approach

Finite element method [6,7] is employed to construct numerical solution of desired problem. It is described under.

Step 1: Firstly, the problem domain is transformed into a finite number of elements and derived linear type polynomial over each element. Weak form can be achieved from strong form using weighted residual function. Weighted residuals [6,7] are derived as

$$\int_{\eta_e}^{\eta_{e+1}} w_1[F' - H]\,d\eta = 0, \int_{\eta_e}^{\eta_{e+1}} w_2[G' - T]\,d\eta = 0, \tag{20}$$

$$\int_{\eta_e}^{\eta_{e+1}} w_3\left[\begin{matrix}\left(1+\frac{1}{\beta}\right)H'' - A_1\left(-n(H+T)H + \frac{n+1}{2}(F+G)H'\right) \\ +\frac{M^2\left(1-\phi_1\right)^{2.5}\left(1-\phi_2\right)^{2.5}}{\left(1+\beta_i\beta_e\right)^2+\left(\beta_e\right)^2}\left(\beta_e T - \left(1+\beta_e\beta_i\right)H\right) + \alpha_1\theta\end{matrix}\right]d\eta = 0, \tag{21}$$

$$\int_{\eta_e}^{\eta_{e+1}} w_4 \left[\begin{array}{c} \left(1+\frac{1}{\beta}\right)T'' + A_1\left(n(H+T)T - \frac{n+1}{2}(F+G)T'\right) + \alpha_2\theta \\ + \frac{M^2(1-\phi_1)^{2.5}(1-\phi_2)^{2.5}}{(1+\beta_i\beta_e)^2+(\beta_e)^2}\left(\beta_e H + (1+\beta_e\beta_i)T\right) \end{array} \right] d\eta = 0, \tag{22}$$

$$\int_{\eta_e}^{\eta_{e+1}} w_5 \left[\begin{array}{c} \theta'' + \frac{k_f}{k_{TH}} \frac{PrEcM^2}{(1+\beta_i\beta_e)^2+(\beta_e)^2}\{(H)^2+(H)^2\} \\ -\frac{k_f(\rho c_p)_{TH}}{k_{TH}(\rho c_p)_f} Pr\left\{\frac{n+1}{2}\theta'(F+G) - n\theta(H+T)\right\} \end{array} \right] d\eta = 0. \tag{23}$$

Here, w_3, w_1, w_2, w_4 and w_5 are weighted functions. Unknown variables and shape functions [6] are defined as

$$F = \sum_{j=1}^{2} F_i\psi_j, T = \sum_{j=1}^{2} T_i\psi_j, G = \sum_{j=1}^{2} G_i\psi_j, H = \sum_{j=1}^{2} H_i\psi_j, \theta = \sum_{j=1}^{2} \theta_i\psi_j, \tag{24}$$

$$\psi_j = (-1)^{i-1}\left(\frac{\eta-\eta_{j-1}}{\eta_i-\eta_{j-1}}\right). \tag{25}$$

Step 2: Boundary integral vectors, stiffness matrices and force vectors are derived. After it, the global stiffness matrix is derived. In additionally, Picard linearization approach is utilized for achieving linear form of algebraic equations. Derivation of stiffness elements are

$$K_{ij}^{11} = \int_{\eta_e}^{\eta_{e+1}} \psi_i\left(\frac{d\psi_j}{d\eta}\right) d\eta, K_{ij}^{13} = -\int_{\eta_e}^{\eta_{e+1}} \psi_i\left(\frac{d\psi_j}{d\eta}\right) d\eta, K_{ij}^{12} = K_{ij}^{14} = K_{ij}^{15} = 0, \tag{26}$$

$$K_{ij}^{21} = \int_{\eta_e}^{\eta_{e+1}} \psi_i\left(\frac{d\psi_j}{d\eta}\right) d\eta, K_{ij}^{24} = -\int_{\eta_e}^{\eta_{e+1}} \psi_i\left(\frac{d\psi_j}{d\eta}\right) d\eta, K_{ij}^{22} = K_{ij}^{23} = K_{ij}^{25} = 0, \tag{27}$$

$$K_{ij}^{33} = \int_{\eta_e}^{\eta_{e+1}} \left[\begin{array}{c} -\left(1+\frac{1}{\beta}\right)\frac{d\psi_i}{d\eta}\frac{d\psi_j}{d\eta} - A_1\left(-n(\overline{H}+\overline{T})\psi_i\psi_j + \frac{n+1}{2}(\overline{F}+\overline{G})\psi_i\psi_j\right) \\ -\frac{M^2(1-\phi_1)^{2.5}(1-\phi_2)^{2.5}}{(1+\beta_i\beta_e)^2+(\beta_e)^2}\left((1+\beta_e\beta_i)\psi_i\psi_j\right) \end{array} \right] d\eta, \tag{28}$$

$$K_{ij}^{34} = \int_{\eta_e}^{\eta_{e+1}} (\beta_e\psi_i\psi_j) d\eta, K_{ij}^{35} = \int_{\eta_e}^{\eta_{e+1}} \alpha_1(\psi_i\psi_j) d\eta, K_{ij}^{31} = 0, K_{ij}^{32} = 0, B_i^5 = 0, \tag{29}$$

$$K_{ij}^{34} = \int_{\eta_e}^{\eta_{e+1}} \left[\begin{array}{c} -A_1\left(n(\overline{H}+\overline{T})\psi_i\psi_j - \frac{\left((\overline{F}+\overline{G})\psi_i\frac{d\psi_j}{d\eta}\right)^{n+1}}{2} \right) \\ -\frac{M^2(1-\phi_1)^{2.5}(1-\phi_2)^{2.5}}{(1+\beta_i\beta_e)^2+(\beta_e)^2}\left((1+\beta_e\beta_i)\psi_i\psi_j\right) \end{array} \right] d\eta, B_i^4 = 0, K_{ij}^{42} = 0, \tag{30}$$

$$K_{ij}^{55} = \int_{\eta_e}^{\eta_{e+1}} \left[\begin{array}{c} -\left(1+N_r\left(1+(\theta_\omega-1)\right)^3\right)' 3\overline{\theta}'^2 \frac{d\psi_i}{d\eta}\frac{d\psi_j}{d\eta} - \frac{k_f(\rho c_p)_{TH}}{k_{TH}(\rho c_p)_f} n(\overline{H}+\overline{T})\psi_i\psi_j \\ -\frac{k_f(\rho c_p)_{TH}}{k_{TH}(\rho c_p)_f} Pr\bar{G}\psi_i\frac{d\psi_j}{d\eta} + \frac{k_f(\rho c_p)_{TH}}{k_{TH}(\rho c_p)_f} Pr\left(\frac{n+1}{2}\right)\bar{F}\psi_i\frac{d\psi_j}{d\eta} \end{array} \right] d\eta, \tag{31}$$

$$K_{ij}^{53}=\int_{\eta_e}^{\eta_{e+1}}\left[\frac{k_f}{k_{TH}}\frac{PrEcM^2}{\left(1+\beta_i\beta_e\right)^2+\left(\beta_e\right)^2}\overline{H}\psi_i\psi_j\right]d\eta,\ K_{ij}^{41}=K_{ij}^{51}=0,K_{ij}^{52}=0,B_i^1=0,K_{ij}^{43}=0, \tag{32}$$

$$K_{ij}^{54}=\int_{\eta_e}^{\eta_{e+1}}\left[\frac{k_f}{k_{TH}}\frac{PrEcM^2}{\left(1+\beta_i\beta_e\right)^2+\left(\beta_e\right)^2}\bar{G}\psi_i\psi_j\right]d\eta,B_i^2=0,B_i^3=0,K_{ij}^{35}=\int_{\eta_e}^{\eta_{e+1}}\alpha_1\left(\psi_i\psi_j\right)d\eta, \tag{33}$$

Step 3: System of linear equations is solved in form of iteratively under numerically tolerance (10^{-5}). Convergence and error analysis is mentioned below

$$Err=\left|\delta^i-\delta^{i-1}\right|,Max\left|\delta^i-\delta^{i-1}\right|\leq 10^{-8}. \tag{34}$$

Step 4: MAPLE 18 is used to design programming of finite element approach. Mesh free study is recorded in Table 2. Flow chart of numerical methodology is addressed by Figure 3. Validation results of present model is verified with already published work [24] considering absence of ternary hybrid nanofluid, power law index number, Darcy's Forchheirmer model and Casson fluid. Validation of numerical results with published work is mentioned in Table 3.

Table 2. Numerical study of mesh free analysis [6] for $F'\left(\frac{\eta_{max}}{2}\right)$, $G'\left(\frac{\eta_{max}}{2}\right)$ and $\theta\left(\frac{\eta_{max}}{2}\right)$.

e	$F'\left(\frac{\eta_{max}}{2}\right)$	$G'\left(\frac{\eta_{max}}{2}\right)$	$\theta\left(\frac{\eta_{max}}{2}\right)$
30	0.5172614186	0.4141116019	0.5331053851
60	0.5009743321	0.3991196957	0.5166109650
90	0.4955010944	0.3940814743	0.5110865969
120	0.4927563199	0.3915549156	0.5083195950
150	0.4911066420	0.3900362436	0.5066578927
180	0.4900077513	0.3890241819	0.5055494665
210	0.4892201185	0.3882992913	0.5047574611
240	0.4886298879	0.3877558788	0.5041632925
270	0.4881717384	0.3873337477	0.5037009996
300	0.4888027764	0.3879944431	0.5033311740

Table 3. Validation of present problem for wall shear stresses with published study [24] considering $n=0,\phi_1=0,M=0,\phi_2=0,\phi_3=0,\beta\to\infty,\epsilon=0,Fr=0$.

n	λ	Khan et al. [24]	present results for $-F''(0)$	Khan et al. [24]	present results for $-G''(0)$
	0.0	1.0	1.0	0.0	0.0
1	0.5	1.224745	0.2210013530	0.612372	0.6124360703
	1.0	1.414214	0.4111910216	1.414214	0.4145020304
	0.0	1.624356	0.6238906653	0.0	0.0
3	0.5	1.989422	0.9893026033	0.994711	0.9950661609
	1.0	2.297182	0.2969018879	2.297182	2.2960670811

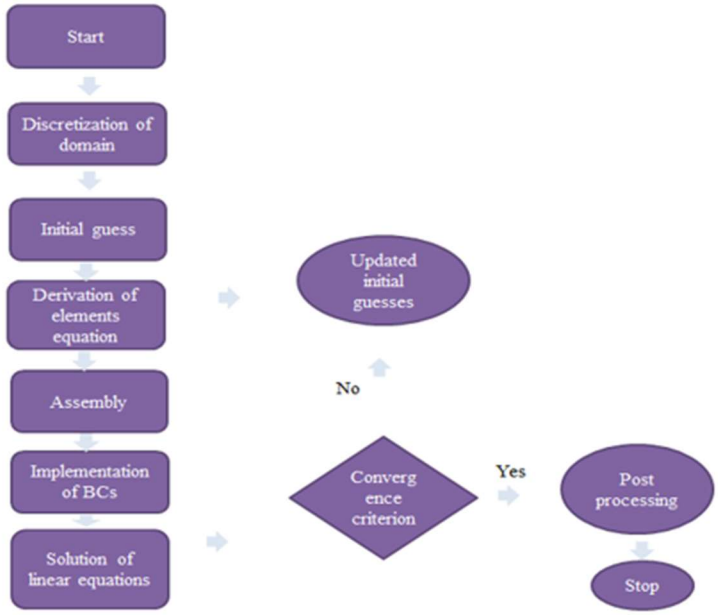

Figure 3. Flow diagram of solution approach.

4. Results and discussion consequences

The parametric study is captured to determine flow behavior and transport of thermal energy into a mixture of ternary hybrid nanoparticles in base and working fluids. The graphical outcomes are displayed in Figures 4–12. It is noticed that ternary hybrid nanofluid is a mixture of aluminum dioxide, titanium dioxide, silicon dioxide in base fluid and working fluid. Hybrid nanofluid is considered a mixture of silicon dioxide, titanium dioxide while nanofluid is a mixture of titanium dioxide in Casson fluid. In additionally, thermal and velocity fields are plotted versus different parameters implementing ranges of $0.5 \leq \beta \leq 4$, $0.1 \leq n \leq 3$, $0.0 \leq M \leq 2.0$, $,0.0 \leq \beta_e \leq 3.0$, $,0.0 \leq \beta_i \leq 4.0$, $,204 \leq Pr \leq 208$, $0.0 \leq Ec \leq 3.0$, $0.0 \leq \alpha_1 \leq 1.5$, $0.0 \leq \phi_1 \leq 0.04$, $0.0 \leq \lambda \leq 0.5$, $0.0 \leq \phi_2 \leq 0.07$, $0.0 \leq \phi_2 \leq 0.07$, $0.0 \leq \phi_3 \leq 0.06$, $0.0 \leq \alpha_1 \leq 2.0$, $0.0 \leq \epsilon \leq 1.5$, $0.0 \leq Fr \leq 3.0$, $0.0 \leq N_r \leq 3.0$ and $0.0 \leq \theta_\omega \leq 2.0$.

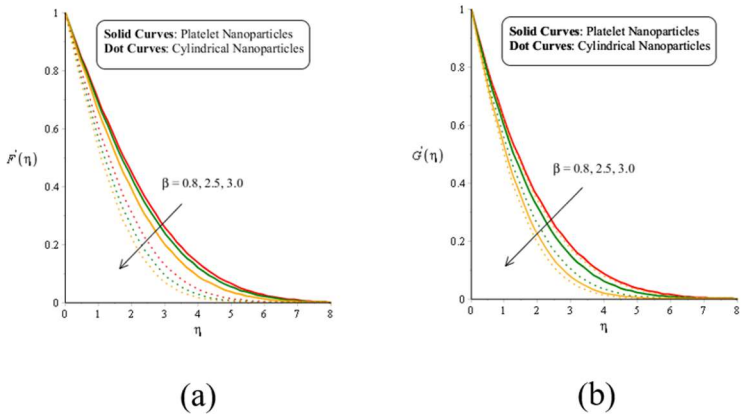

(a) (b)

Figure 4. Distribution in velocity fields with β.

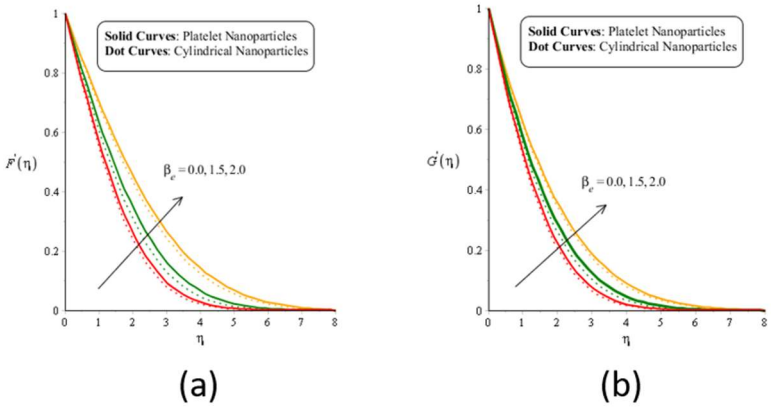

Figure 5. Distribution in velocity fields with β_e.

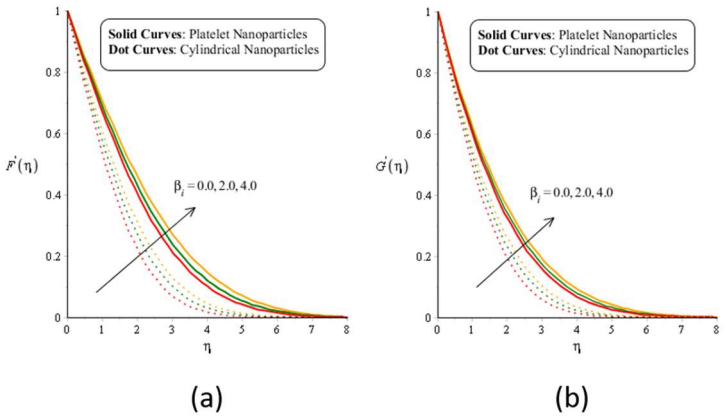

Figure 6. Distribution in velocity fields with β_i.

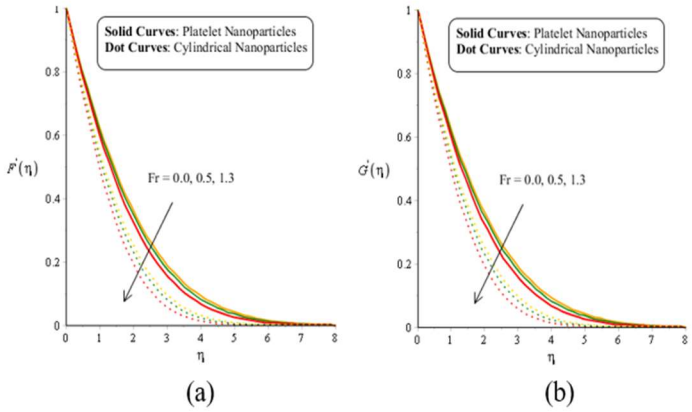

Figure 7. Distribution in velocity fields with Fr.

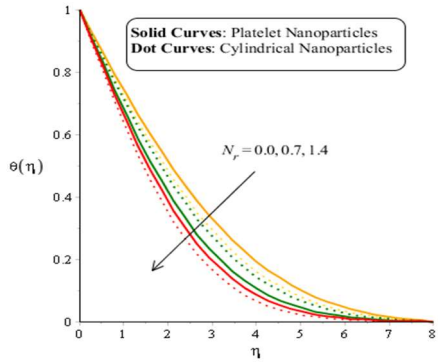

Figure 8. Distribution in thermal field with N_r.

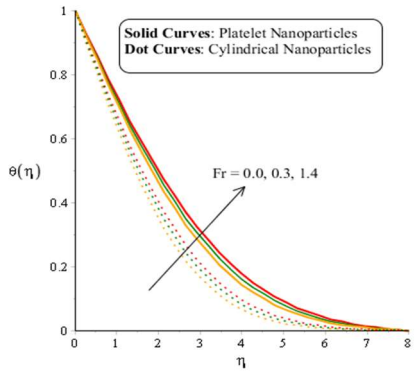

Figure 9. Distribution in thermal field with Fr.

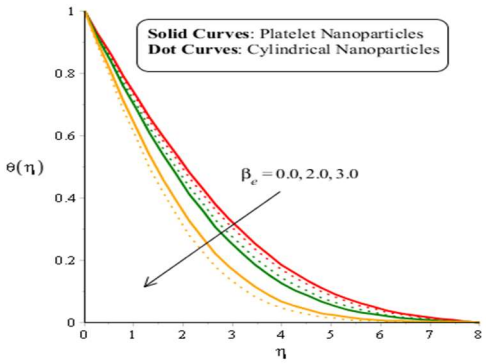

Figure 10. Distribution in thermal field with β_e.

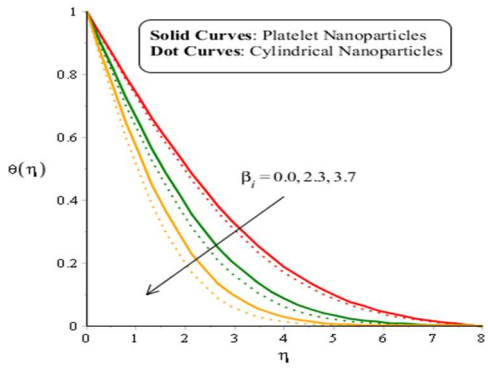

Figure 11. Distribution in thermal field with β_i.

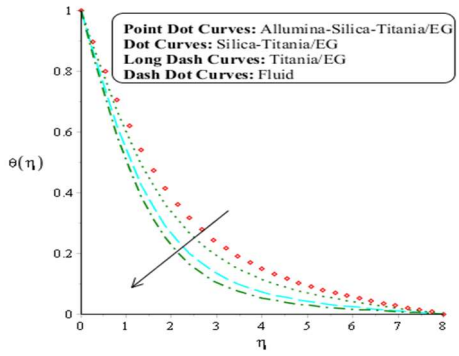

Figure 12. Comparison influences among fluid, hybrid nanofluid, trihybrid nanofluid and nanofluid.

Figures 4–7 are plotted to determine the effect of several parameters on flow involving dispersion of ternary hybrid nanoparticles. It is visualized that platelet nanoparticles are represented by solid curves on graphs and dot curves are associated with cylindrical nanoparticles on graphs. Figure 4 clearly reveal that there is reduction into flow (y- and x-directions) when β is changed. The effect of the Casson parameter for cylindrical nanoparticles is less than the effect of the Casson number for platelet nanoparticles. This effect is created using concept of Casson fluid in momentum equations whereas existence of β is formulated considering tensor of Casson fluid in momentum equations. Flow becomes reduced in y- and x-directions because of β is appeared in form of $\frac{1}{\beta}$. Therefore, an inverse proportional relation can be investigated versus velocity fields. Consequently, flow slows down in terms of y- and x-directions. Casson fluid behaves as a shear thinning and non-Newtonian liquid. Flow becomes significant for higher values of β rather flow for minimize values of β. Thickness for momentum boundary layers is declined when β is gradually enhanced. It is studied that current analysis is transformed into Newtonian model for $\beta \to \infty$ while other values of β is case of non-Newtonian model. In momentum equation, β occurs in the denominator. Hence, an inclination in β results velocity field is enhanced. Role β_e (Hall parameter) is predicted on flow

behavior in term of y- and x-directions. An enhancement is studied into flow (x-and y-direction) versus variation in β_e. It is dimensionless parameter which is formulated using the theory of generalized Ohm's law in current analysis. Further, flow for platelet nanoparticles is produced significantly rather than flow for cylindrical particles. Figure 5 visualize the role of ion slip number (β_i) on velocity fields in terms of y- and x-directions. Similar impact is conducted when β_i is increased. It is observed that ethylene glycol was predicted as plasma and its behavior of flow is exposed as a non-uniform magnetic field. An interaction among plasma and magnetic field produces ion slip and Hall currents which is responsible for ion slip and Hall forces. Applied magnetic field is opposite against action of ion slip and Hall forces. Hence, Lorentz force reduces when β_e and β_i are increased. Physically, magnetic field was placed perpendicular along the z-direction of the surface and against flow. Therefore, flow was reduced by applying higher values of Lorentz force because Lorentz force is addressed as opposite against applied magnetic field. Thickness based on flow curves for the case of platelet nanoparticles is higher than thickness generated by cylindrical nanoparticles. Role of Fr on flow in y- and x-directions is addressed by Figure 7. It was found that velocity distribution in y- and x-directions is decreased in presence of higher numerical values of Fr. It is noticed that Fr is dimensionless parameter which is produced considering Forchheirmer-porous theory. Mathematically, Fr is inversely proportional versus velocity field. Consequently, an inclination in Fr results flow increases in y- and x-directions. Thickness for the momentum layers is declined when Fr is changed. Flow for case of $Fr = 0$ is greater than flow for case $Fr \neq 0$.

Figures 8–11 reveal impact of temperature profile carrying three kind nanoparticles having cylindrical and platelet shapes against change in N_r, Fr, β_e and β_i. Reduction into temperature versus implication of N_r has been estimated by Figure 8. Highest performance of thermal process for case of platelet nanoparticles has been obtained rather than for cylindrical particles. It is addressed that N_r is termed as dimensionless which is produced using the concept of non-uniform thermal radiation in energy equation. It was noticed that thermally energy reduces when N_r is distributed. Physically, heat energy moves away from $z = 0$ along with thermal radiations. Therefore, temperature decreases at walls of plate. Thickness of thermally layers for case of platelet nanoparticles is greater than thermally thickness for case of cylindrical nanoparticles. Observations of Fr on thermally field was investigated by Figure 9 including ternary hybrid nanoparticles. Maximum production of thermal field was estimated versus distribution in Fr. Thermal enhancement for the case $Fr = 0$ is less than thermal enhancement for case of $Fr \neq 0$. Thermal production for cylindrical particles in presence of variable thermal conductivity is less than thermal production for platelet particles. Figures 10 and 11 are plotted to estimate distribution into thermal energy using parameters regarding ion slip (β_i) and Hall parameters (β_e). Reduction into thermal distribution was visualized using higher values of ion slip (β_i) and Hall parameters (β_e). Ion slip (β_i) and Hall (β_e) are opposite against Lorentz force. Further, collision rate into nanoparticles is inversely directly proportional to ion slip and Hall forces result in reduction into magnetic intensity. This reduction in magnetic intensity produces declination on thermal profile. Platelet nanoparticles experience significant thermal energy rather than experience of thermal energy for cylindrical nanoparticles. Physically, β_i and β_e are associated in the denominator of the Joule heating term in the energy equation. Consequent, heat energy generates because of the Joule heating process. Figure 12

reveals comparison analysis among alumina-silica-titania nanoparticles/EG, silica-titania nanoparticles/EG, silica-titania nanoparticles/EG, titania nanoparticles/EG and working fluid. It was observed that alumina-silica-titania nanoparticles/EG experiences higher thermal energy rather than for the cases of silica-titania nanoparticles/EG, silica-titania nanoparticles/EG, titania nanoparticles/EG and working fluid. Therefore, ternary hybrid nanofluid is observed as most significant for producing maximum production of thermal energy as well as reduction in thermal energy.

Table 4 is prepared to determine production of wall shear stresses and thermal rate using change in Hall parameter, magnetic parameter, ion slip parameter, Casson parameter and Fr. It was numerically investigated that production of thermal rate ingresses when Hall parameter, magnetic parameter, ion slip parameter are changed. However, the same behavior is investigated versus β and thermal rate decreases versus change in Fr. Wall shear stresses are inversely proportional against distribution in ion slip parameter, Casson number and Hall parameter. But inverse behavior for case of wall shear stresses is estimated when Lorentz force is changed.

Table 4. Numerically behavior of wall shear stresses and Nusselt number [26] with distribution in Fr, β, M, β_e and β_i.

Parameters	Distribution in parameters	$-Re^{1/2}Cf$	$-Re^{1/2}Cg$	$-Re^{-1/2}Nu$
	0.0	0.2625008163	0.4236006667	1.652101988
Fr	0.5	0.2701304207	0.4424323033	1.634134933
	1.4	0.2905110133	0.4903136669	1.610193943
	1.5	0.2192892414	0.2595109874	1.751988063
β	2.0	0.2403202308	0.2706220343	1.730933030
	3.5	0.2700293493	0.2903119971	1.711018177
	0.0	0.2233998059	0.2824407947	1.747439085
M	0.6	0.2346098044	0.2903302023	1.754403388
	1.2	0.2472144519	0.3184495583	1.780274025
	0.0	0.2437500727	0.2688997575	1.754913084
β_e	0.4	0.2242905241	0.2214389298	1.764917691
	0.8	0.2146742280	0.2116991296	1.794919036
	0.0	0.2741394839	0.2805626046	1.754917615
β_i	0.4	0.2341541906	0.2304551660	1.7843013073
	0.8	0.2141711628	0.2202741977	1.7899183003

5. Conclusions

Thermal aspects of Casson fluid containing ternary hybrid nanofluid over stretching sheet utilizing Darcy's Forchheirmer theory are addressed. Various shapes regarding nanoparticles (platelet, cylindrical and spherical) are implemented in EG. Thermal radiation (non-linear) is utilized in the energy equation considering effects of viscous dissipation and variable wall velocity. Performance of several parameters on flow and temperature profile is addressed and numerical study is tackled by FEM. Key findings of the problem are listed below.

- Hall and ion slip numbers play a remarkable role in controlling momentum and thermal boundary layers. However, declination into motion has been investigated versus β and Fr.

- Temperature decreases against variation in β_e and β_i but opposite trend is noticed in thermal layers against distribution in Fr.
- Ethylene glycol is studied as partially ionized and shear thinning and its interaction with magnetic field produces ion slip and Hall currents. Due to this process, EG experiences ion slip and Hall forces which are against Lorentz force. Therefore, flow of EG was accelerated versus change in β_e and $\beta_{i.}$
- Convergence of current analysis is ensured using finite element methodology.
- Maximum production for thermal energy can be achieved rather than nanofluid and hybrid nanofluid. This process is applicable in coolants (in automobiles), fuel dynamics, solar system, microelectronics, temperature reduction, cooling process and pharmaceutical process.
- It was included that platelet nanoparticles experience more heat energy rather than thermal energy for cylindrical nanoparticles. Similar behavior was analyzed in velocity fields.
- Nusselt number increases versus change in ion slip, Hall and M parameters but thermal rate decreases versus distribution in Fr.

Acknowledgements

This research was supported by the Postdoctoral Research Fellowship Training Program from Khon Kaen University (PD2565-02-05).

Conflicts of interest

The authors declare that they have no conflicts of interest.

References

1. N. Casson, *A flow equation for pigment-oil suspensions of the printing ink type*, Rheology of disperse systems, 1959.
2. I. Chabani, F. Mebarek-Oudina, A. A. I. Ismail, MHD flow of a hybrid nano-fluid in a triangular enclosure with zigzags and an elliptic obstacle, *Micromachines*, **13** (2022), 224. https://doi.org/10.3390/mi13020224
3. Y. M. Chu, S. Bashir, M. Ramzan, M. Y. Malik, Model-based comparative study of magnetohydrodynamics unsteady hybrid nanofluid flow between two infinite parallel plates with particle shape effects, *Math. Method. Appl Sci*., 2022. https://doi.org/10.1002/mma.8234
4. F. Selimefendigil, H. F. Öztop, M. Afrand, Shape effects of TEG mounted ventilated cavities with alumina-water nanofluids on the performance features by using artificial neural networks, *Eng. Anal. Bound. Elem.*, **140** (2022), 79–97. https://doi.org/10.1016/j.enganabound.2022.04.005
5. S. Saleem, I. L. Animasaun, S. J. Yook, Q. M. Al-Mdallal, N. A. Shah, M. Faisal, Insight into the motion of water conveying three kinds of nanoparticles shapes on a horizontal surface, Significance of thermo-migration and Brownian motion, *Surf. Interfaces*, **30** (2022), 101854. https://doi.org/10.1016/j.surfin.2022.101854

6. S. Saleem, D. Gopal, N. A, Shah, N. Feroz, N. Kishan, J. D. Chung, et al., Modelling entropy in magnetized flow of eyring-powell nanofluid through nonlinear stretching surface with chemical reaction: A finite element method approach, *Nanomaterials*, **12** (2022), 1811. https://doi.org/10.3390/nano12111811
7. E. A. Algehyne, E. R. El-Zahar, S. H. Elhag, F. S. Bayones, U. Nazir, M. Sohail, et al., Investigation of thermal performance of Maxwell hybrid nanofluid boundary value problem in vertical porous surface via finite element approach, *Sci. Rep*., **12** (2022), 2335. https://doi.org/10.1038/s41598-022-06213-8
8. M. Imran, S. Yasmin, H. Waqas, S. A. Khan, T. Muhammad, N. Alshammari, et al., Computational analysis of nanoparticle shapes on hybrid nanofluid flow due to flat horizontal plate via solar collector, *Nanomaterials*, **12** (2022), 663. https://doi.org/10.3390/nano12040663
9. M. Sohail, U. Nazir, S. Naz, A. Singh, K. Mukdasai, M. A. Ali, et al., Utilization of Galerkin finite element strategy to investigate comparison performance among two hybrid nanofluid models, *Sci. Rep.*, ***12*** (2022), 18970. https://doi.org/10.1038/s41598-022-22571-9
10. U. Khan, F. Mebarek-Oudina, A. Zaib, A. Ishak, S. Abu Bakar, E. S. M Sherif, et al., An exact solution of a Casson fluid flow induced by dust particles with hybrid nanofluid over a stretching sheet subject to Lorentz forces, *Wave. Random Complex*, **2022** (2022), 1–14. https://doi.org/10.1080/17455030.2022.2102689
11. K. Sarada, F. Gamaoun, A. Abdulrahman, S. O. Paramesh, R. Kumar, G. D. Prasanna, et al., Impact of exponential form of internal heat generation on water-based ternary hybrid nanofluid flow by capitalizing non-Fourier heat flux model, *Case Stud. Therm. Eng.*, **38** (2022), 102332. https://doi.org/10.1016/j.csite.2022.102332
12. U. Nazir, M. Sohail, P. Kumam, K. Sitthithakerngkiet, A. A. A. Mousa, M. J. Khan, et al., A dynamic assessment of various non-Newtonian models for ternary hybrid nanomaterial involving partially ionized mechanism, *Sci Rep.*, **12** (2022), 10306. https://doi.org/10.1038/s41598-022-14312-9
13. A. Dezfulizadeh, A. Aghaei, A. Hassani Joshaghani, M. M. Najafizadeh, Exergy efficiency of a novel heat exchanger under MHD effects filled with water-based Cu-SiO_2-MWCNT ternary hybrid nanofluid based on empirical data, *J. Therm. Anal. Calorim.*, **147** (2022), 4781–4804. https://doi.org/10.1007/s10973-021-10867-3
14. A. S. Oke, Heat and mass transfer in 3D MHD flow of EG-based ternary hybrid nanofluid over a rotating surface, *Arab. J. Sci. Eng*., **47** (2022), 16015–16031. https://doi.org/10.1007/s13369-022-06838-x
15. W. Xiu, I. L. Animasaun, Q. M. Al-Mdallal, A. K. Alzahrani, T. Muhammad, Dynamics of ternary-hybrid nanofluids due to dual stretching on wedge surfaces when volume of nanoparticles is small and large: forced convection of water at different temperatures, *Int. Commun. Heat Mass,* **137** (2022), 106241. https://doi.org/10.1016/j.icheatmasstransfer.2022.106241
16. I. L. Animasaun, K. K. Asogwa, Significance of suction and dual stretching: Comparative analysis between the dynamics of water-based alumina nanoparticle aggregation with water-based cupric nanoparticle aggregation, *J. Nigerian Math. Soc.*, **40** (2022), 161–181.
17. G. Rasool, A. Shafiq, Y. M. Chu, M. S. Bhutta, A. Ali, Optimal homotopic exploration of features of cattaneo-christov model in second grade nanofluid flow via Darcy-Forchheimer medium subject to viscous dissipation and thermal radiation, *Comb. Chem. High T. Scr*., **25** (2022), 2485–2497. https://doi.org/10.2174/1386207324666210903144447

18. M. U. Ashraf, M. Qasim, A.Wakif, M. I. Afridi, I. L. Animasaun, A generalized differential quadrature algorithm for simulating magnetohydrodynamic peristaltic flow of blood-based nanofluid containing magnetite nanoparticles: A physiological application, *Numer. Meth. Part. D. E.*, **38** (2022), 666–692. https://doi.org/10.1002/num.22676
19. L. Hendraningrat, O. Torsæter, Metal oxide-based nanoparticles: revealing their potential to enhance oil recovery in different wettability systems, *Appl. Nanosci.*, **5** (2015), 181–199. https://doi.org/10.1007/s13204-014-0305-6
20. Y. Q. Song, B. D. Obideyi, N. A. Shah, I. L. Animasaun, Y. M. Mahrous, J. D. Chung, Significance of haphazard motion and thermal migration of alumina and copper nanoparticles across the dynamics of water and ethylene glycol on a convectively heated surface, *Case Stud. Therm. Eng.*, **26** (2021), 101050. https://doi.org/10.1016/j.csite.2021.101050
21. I. L. Animasaun, N. A. Shah, A. Wakif, B. Mahanthesh, R. Sivaraj, O. K. Koriko, *Ratio of momentum diffusivity to thermal diffusivity: Introduction, meta-analysis, and scrutinization.*, CRC Press, 2022.
22. I. L. Animasaun, O. K. Koriko, K. S. Adegbie, H. A. Babatunde, R. O. Ibraheem, N. Sandeep, et al., Comparative analysis between 36 nm and 47 nm alumina-water nanofluid flows in the presence of Hall effect, *J. Therm. Anal. Calorim.*, **135** (2019), 873–886. https://doi.org/10.1007/s10973-018-7379-4
23. A. A. Farooq, M. Kahshan, S. Saleem, M. Rahimi-Gorji, F. S. Al-Mubaddel, Entropy production rate in ciliary induced flows through cylindrical tubules under the consequences of Hall effect, *J. Taiwan Inst. Chem. E.*, **120** (2021), 207–217. https://doi.org/10.1016/j.jtice.2021.03.024
24. J. A. Khan, M. Mustafa, T. Hayat, A. Alsaedi, On three-dimensional flow and heat transfer over a non-linearly stretching sheet: analytical and numerical solutions, *PloS one.*, **9** (2014), e107287. https://doi.org/10.1371/journal.pone.0107287
25. M. Maurer, C. Kessler, Identification and quantification of ethylene glycol and diethylene glycol in plasma using gas chromatography-mass spectrometry, *Arch. Toxicol.,* **62** (1988), 66–69. https://doi.org/10.1007/BF00316260
26. A. Mariano, M. J. Pastoriza-Gallego, L. Lugo, A. Camacho, S. Canzonieri, M. M. Piñeiro, Thermal conductivity, rheological behaviour and density of non-Newtonian ethylene glycol-based SnO_2 nanofluids, *Fluid Phase Equilibr.*, **337** (2013), 119–124. https://doi.org/10.1016/j.fluid.2012.09.029
27. I. Tlili, Impact of thermal conductivity on the thermophysical properties and rheological behavior of nanofluid and hybrid nanofluid, *Math. Sci.,* 2022. https://doi.org/10.1007/s40096-021-00377-6
28. I. L. Animasaun, S. J. Yook, T. Muhammad, A. Mathew, Dynamics of ternary-hybrid nanofluid subject to magnetic flux density and heat source or sink on a convectively heated surface, *Surf. Interfaces*, **28** (2022), 101654. https://doi.org/10.1016/j.surfin.2021.101654

AIMS Press